ACS APPLIED MATERIALS & INTERFACES

www.acsami.org

Research Article

Charge Transfer in Nanowire-Embedded PEDOT:PSS and Planar Heterojunction Solar Cells

Joseph P. Thomas, Qiuyu Shi, Marwa Abd-Ellah, Lei Zhang, Nina F. Heinig, and Kam Tong Leung*

Cite This: *ACS Appl. Mater. Interfaces* 2020, 12, 11459–11466

Read Online

ACCESS | Metrics & More | Article Recommendations | Supporting Information

ABSTRACT: Hybrid metallic nanowire-embedded, highly conductive poly(3,4-ethylenedioxy thiophene):polystyrenesulfonate (PEDOT:PSS) with synergetic properties is indispensable for enhancing the performances of conductive polymer-based electronic devices. Here, we report embedment of silver nanowires (AgNWs), with diameter ∼100 nm and a high concentration (500 mg/mL) of nanowires dispersed in either ethanol or isopropanol, in PEDOT:PSS and compare the effects of the nanowire-dispersing solvents as well as its thicker diameter and high concentration on the overall properties and particularly its charge transfer characteristics and planar heterojunction solar cell (HSC) properties. Furthermore, electrostatic force microscopy is applied to elucidate the direct charge transfer from AgNWs to the PEDOT:PSS matrix. The AgNW-embedded PEDOT:PSS-based planar HSCs show a very high open-circuit voltage of over 638 mV and a high power conversion efficiency greater than 15.3% and without any significant influence from the AgNW dispersing solvents. While charge transfer in PEDOT:PSS without AgNWs occurs through the conducting PEDOT grains, enhanced charge transfer is realized in AgNW-embedded PEDOT:PSS with charge transport from PEDOT grains to AgNWs and then to PEDOT grains before reaching the top electrode in the HSC. The AgNW-embedded PEDOT:PSS hybrid materials pave a simple way to enhance the charge transfer performance in not only HSCs but also other hybrid or heterojunction electronics.

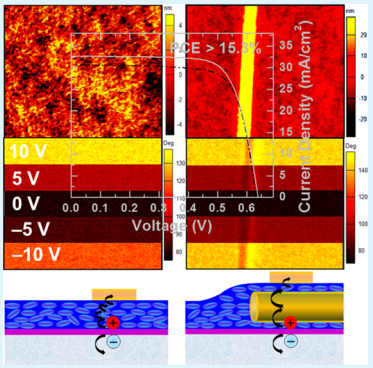

KEYWORDS: *conducting polymer, poly(3,4-ethylenedioxy thiophene):polystyrenesulfonate or PEDOT:PSS, silver nanowire, electrostatic force microscopy, charge transfer, heterojunction solar cell*

INTRODUCTION

The aqueous-based conducting polymer poly(3,4-ethylenedioxy thiophene):poly(styrenesulfonate) (PEDOT:PSS) has found several applications in polymer-based electronic devices, including all polymer and heterojunction solar cells (HSCs).[1−7] The cost-effective device fabrication processes, such as spin-coating, can be used to generate homogeneous PEDOT:PSS thin films on different substrates after the addition of appropriate surfactants,[8−13] which makes PEDOT:PSS highly desirable for inexpensive device fabrication. Significant efforts to further enhance the conductivity of this polymer have been carried out by various methods including solvent addition and post-surface treatments. The addition of appropriate cosolvents[8,11,12] has been reported to be one of the most popular methods among the many different approaches to improve its conductivity. Higher conductivities obtained with surface treatments,[14−17] such as the acid treatment,[16] have also been reported. However, these procedures are quite complex and they become less practical and increase device manufacturing cost. Among the different solvent addition approaches to improve the properties of PEDOT:PSS, the simple and most viable method to achieve the highest conductivities has been cosolvent addition, which involves the addition of appropriate amounts of either ethylene glycol (EG)[8,18] or mixed cosolvents (EG and methanol)[12] in PEDOT:PSS. Typically, cosolvent addition facilitates the formation of PEDOT microstructure grains with highly conducting quinoid chains preferably over its less conducting benzoid counterparts in the PEDOT:PSS matrix.[19−21] The mixed cosolvent process has also been found to enhance the separation and removal of the insulating PSS from the PEDOT:PSS matrix, in addition to facilitating the formation of highly conducting quinoid chains.[12]

Alternate approaches to enhance the conductivity of PEDOT:PSS by forming hybrid structures, such as adding nanoparticles or nanowires into the solution or in between or on top of the films, have also been attempted.[5,22−26] Recently, we reported the enhancement of PEDOT:PSS conductivity and HSC performance achieved by efficient embedment of AgNWs with an average diameter of 25 nm in PEDOT:PSS.[23] AgNWs have been chosen for embedding in PEDOT:PSS because of its highly conductive nature, ease of fabrication,

Received: October 27, 2019
Accepted: February 14, 2020
Published: February 14, 2020

https://dx.doi.org/10.1021/acsami.9b19400
ACS Appl. Mater. Interfaces 2020, 12, 11459−11466

flexibility, and commercial availability. As direct addition of AgNWs into the PEDOT:PSS solution is found to cause structural deterioration of AgNWs, more effective embedment can be carried out by premixing the AgNWs in the mixed cosolvent prior to adding to the PEDOT:PSS solution.[23] Further development of more effective embedment methods of nanoparticles or nanowires in PEDOT:PSS for fabricating highly conductive hybrid structures is important to exploit the widespread use of these hybrid materials in not only HSCs but also other electronic devices.

Planar HSCs with high efficiencies are of special interest in building inexpensive solar cells because they can be achieved by simple fabrication routes. The power conversion efficiency (PCE) of HSCs made of p-type PEDOT:PSS and n-type Si has been recently reported to exceed 15%.[27,28] However, the high efficiencies of most of these HSCs made on planar substrates (i.e., without complex substrate structure modifications) have been obtained by employing antireflective coatings,[29,30] interface engineering that involved tuning the contact properties of silicon substrates,[31,32] and optimizing the PEDOT:PSS properties.[12] Incorporating metallic nanowires, such as AgNWs, in PEDOT:PSS to create hybrid material systems with ultralong (several tens of microns) nanowires as efficient charge transfer conduits can be advantageous in enhancing not only the solar cell properties but also the conducting properties of PEDOT:PSS in general.[23] Efforts to elucidate the charge transport characteristics in this type of hybrid structures could further open up their potential use in fabricating other low-cost high-efficiency electronic devices.

Although HSCs comprising AgNWs (embedded inside or as layers in between) and PEDOT:PSS have been reported, better understanding of how the different dispersing solvents that contain the AgNWs can influence the properties of PEDOT:PSS and HSCs is acutely needed. Such a study can benefit exploiting the development of this technologically important PEDOT:PSS for its widespread use in polymer-based electronic devices. Therefore, in this study, we incorporate AgNWs with diameter ∼100 nm, predispersed in either isopropanol (IPA) or ethanol (EtOH), in PEDOT:PSS, in order to examine its influence on the overall properties of the hybrid films including their charge transfer properties and HSC performance. The use of two different dispersing solutions (i.e., IPA and EtOH) for AgNWs will allow us to determine the effect of these dispersing solutions on the aforementioned properties. Furthermore, a rather high concentration of 500 mg/mL AgNWs (relative to a typical range of 1−5 mg/mL)[23] is chosen for the embedment to obtain higher conductivities with their expected better interconnecting networks. Interestingly, we find that the antireflective properties of PEDOT:PSS films are also enhanced with the embedment of AgNWs as compared to mixed cosolvent-modified PEDOT:PSS films (without AgNWs) on Si substrates. We utilize electrostatic force microscopy (EFM) to study the charge transfer properties between AgNWs and PEDOT:PSS, and the results demonstrate that the AgNWs act as essential charge transfer paths while the AgNW-dispersing solvents produce only minor differences in their charge transfer characteristics. The addition of AgNWs also improves the HSC performance and a high PCE of 15.4% can be obtained for these simple planar cells without the need for any additional post-treatment or elaborate interface engineering.

EXPERIMENTAL SECTION

PEDOT:PSS (PH1000), AgNWs (500 mg/mL dispersed in either IPA or EtOH) with diameter ∼100 nm and length ∼15−30 μm, and all other chemicals were purchased from commercial sources. A 16 wt % of the stock cosolvent mixture of 50 wt % of EG and 50 wt % of methanol (MeOH) was mixed with the PEDOT:PSS solution (filtered through a 0.45 μm PVDF syringe filter) to prepare the EM16 solution.[12,23] Typical solutions prepared with different constituents in this study are schematically shown in Figure S1 (Supporting Information). The optimized 0.25 wt % of suspensions of AgNWs in IPA or EtOH was mixed with the mixed cosolvent prior to adding 16 wt % of the AgNW-suspended mixed cosolvent to the PEDOT:PSS solution (denoted as AgNW−IPA and AgNW−EtOH, respectively).[23] A 0.25 wt % fluorosurfactant (FS-300) was also added to the modified PEDOT:PSS solutions to improve the wettability of the solutions on the substrates.[12,23] The thin films deposited on glass substrates were used for sheet resistance and EFM studies. Planar Si(100) substrates (380 ± 25 μm thick, single side polished, phosphorus-doped, n-type, resistivity of 0.05−0.10 ohm·cm, Virginia Semiconductor Inc.) were used for solar cell device fabrication and for other characterization.[23] The PEDOT:PSS film deposition using spin-coating and other HSC device fabrication steps have been reported elsewhere.[9,23]

The AgNWs and film surface morphologies were examined by scanning electron microscopy (SEM, Zeiss Merlin) and by transmission electron microscopy (TEM, Zeiss Libra 200 MC). The sheet resistances were measured by using the four-point probe method (van der Pauw configuration, Ecopia HMS-5300).[23] The reflectance spectra of the films were obtained in a UV−Vis spectrophotometer (PerkinElmer Lambda 1050). The measurement methods for HSCs have been reported earlier.[7] Chemical-state composition of the AgNWs was analyzed as a function of Ar ion sputtering time (30, 60, 180, and 300 s) by depth-profiling X-ray photoelectron spectroscopy (XPS, Thermo-VG Scientific ESCALab 250). The spectra were obtained using a monochromatic Al Kα source (1486.6 eV), and Casa XPS software was used for peak fitting (after appropriate Shirley background correction) and analysis.[23] The atomic force microscopy (AFM) or EFM measurements were performed in an ambient atmosphere with an Asylum Research Cypher microscope. A Ti/Ir-coated silicon tip (ASYLEC-01-R2) with a resonance frequency at ∼58−97 kHz and a spring constant k ∼ 2.8 N/m was used in AFM or EFM imaging.

RESULTS AND DISCUSSION

A very high concentration of AgNWs (500 mg/mL) with diameter ∼100 nm, dispersed in EtOH or in IPA, is embedded in PEDOT:PSS to study their effect on modifying the overall properties, especially the charge transfer characteristics and HSC efficiency enhancement. An SEM image of typical AgNWs (dispersed in IPA) used for the embedment in PEDOT:PPS is shown in Figure 1a and the corresponding TEM image of a single nanowire is shown in Figure 1b, which confirms that the average diameter of the nanowires is 100 ± 10 nm. Similar results are also observed for the nanowires dispersed in EtOH (Figure S2a,b, Supporting Information). The low-magnification SEM images (Figure S3a,b, Supporting Information) confirm that the ultralong AgNWs in both IPA and EtOH are of several tens of micrometers long. The SEM image of AgNW-embedded PEDOT:PSS in Figure 1c shows the same nanowire morphology as AgNWs before their addition into PEDOT:PSS (Figure 1a), which is also confirmed by the corresponding TEM result (Figure 1d). The ellipsoidal PEDOT grains are also faintly visible between the AgNWs in the TEM image. The chemical structures of PEDOT:PSS with quinoid (center) and benzoid (edges) chains in PEDOT and of the insulating PSS chains, along with

https://dx.doi.org/10.1021/acsami.9b19400
ACS Appl. Mater. Interfaces 2020, 12, 11459−11466

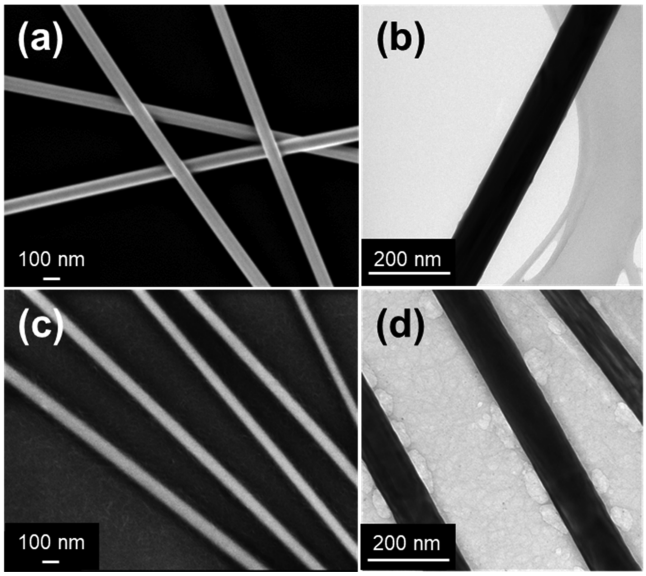

Figure 1. SEM and TEM images of AgNWs (a,b) before and (c,d) after addition to PEDOT:PSS.

those of mixed cosolvent EG and methanol (labelled as EM), solvent IPA or EtOH used for dispersing AgNWs, and the schematic representations of the prepared solutions without and with AgNWs are shown in Figure S1 (Supporting Information). The EM16 solution is prepared for comparison with an optimized 16 wt % of the mixed cosolvent of EG and methanol addition to PEDOT:PSS.[13] Solutions labeled AgNW−IPA and AgNW−EtOH are obtained by preblending optimized 0.25 wt % AgNWs (in the respective dispersing solvents) in the mixed cosolvent solution first prior to adding the AgNW-embedded mixed cosolvent solution to PEDOT:PSS.[23]

The highly conducting metallic nanowires effectively embedded in PEDOT:PSS are expected to improve the conductivity. To evaluate their effects on the conductivity, the PEDOT:PSS films with and without AgNWs are deposited on glass substrates for sheet resistance measurement and charge transfer characterization. The sheet resistance (R_s) measurement (Table S1, Supporting Information) shows a value of 139.0 Ω/□ for the EM16 film (i.e., without the AgNWs). The AgNW−IPA film, obtained by an optimized 0.25 wt % AgNWs dispersed in IPA and then preblended with the mixed cosolvent prior to adding to PEDOT:PSS, is found to show a decrease in R_s to 132.5 Ω/□. In addition, the R_s value for the AgNW−EtOH film, obtained by an optimized 0.25 wt % AgNWs in EtOH preblended with the mixed cosolvent before adding to PEDOT:PSS, is also reduced to 133.5 Ω/□ but is slightly higher than the AgNW−IPA film. It is evident that the embedment of AgNWs in PEDOT:PSS by premixing the NWs in the mixed cosolvent prior to the addition to PEDOT:PSS (AgNW−IPA or AgNW−EtOH) has improved the conducting nature of the hybrid AgNW-PEDOT:PSS films compared to the EM16 film.[23] To verify the conducting nature of the AgNWs, films of AgNWs (separately dispersed in IPA and EtOH) drop-casted directly on glass substrates are also tested and the results show very low sheet resistance values (R_s < 20 Ω/□). It is known from our earlier studies that there is a slight increase in the sheet resistance (R_s > 140 Ω/□) for the PEDOT:PSS film with just the solvent (IPA or EtOH) used to disperse the AgNWs added in PEDOT:PSS, that is, adding aliquot of IPA or EtOH but without any AgNWs to PEDOT:PSS.[23] It is therefore evident that the conductivity enhancement is limited at present by the PEDOT:PSS properties only and it appears not significantly influenced by the dispersing solvents. In addition, nanowires with a diameter that is slightly larger than the PEDOT:PSS film thickness are causing a rougher surface as evidenced from the AFM studies, discussed later.

Figure 2a shows a schematic diagram of a typical HSC with a AgNW-embedded PEDOT:PSS layer on a Si/SiO_x substrate

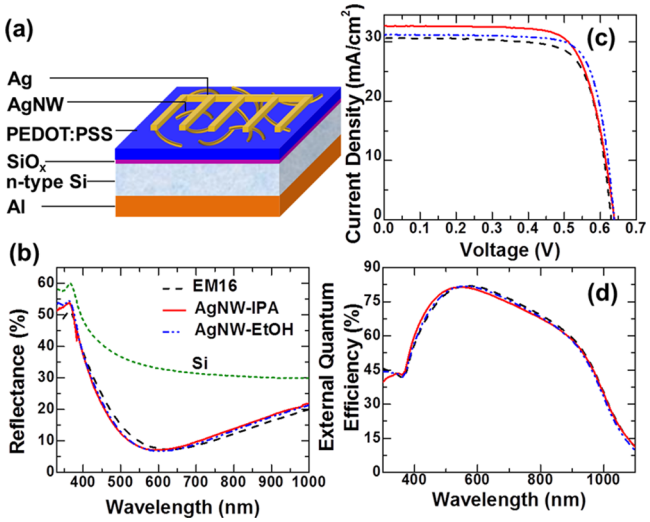

Figure 2. (a) Schematic diagram of a typical HSC with a PEDOT:PSS layer embedded with AgNWs on a Si/SiO_x substrate. (b) Reflectance spectra of AgNW−IPA, AgNW−EtOH, and EM16 films, and (c) current density vs voltage profiles and (d) external quantum efficiency curves of HSCs made from AgNW−IPA, AgNW−EtOH, and EM16 films, all on planar Si/SiO_x substrates.

sandwiched between a comb-shaped Ag top electrode and an Al thin-film bottom electrode. It is known that the inherent antireflective property of the PEDOT:PSS film on a Si/SiO_x substrate can improve the photovoltaic properties. The reflectance spectra of the films (Figure 2b), obtained with and without AgNWs in PEDOT:PSS, on Si/SiO_x substrates along with that of a pristine Si/SiO_x substrate illustrate similar high antireflective properties and the reflectance minima reached below 7.3% near 600 nm for all the films. Furthermore, the reflectance minima of the AgNW−IPA and AgNW−EtOH samples exhibit small blue shifts of ∼39 and ∼24 nm, respectively, relative to the EM16 sample. The slight difference in the shifts of the reflectance minima between the two different AgNW-embedded PEDOT:PSS samples is likely caused by the top surface characteristics and scattering effects, which are evidenced from the AFM topography results. In addition, the transmittance spectra of the PEDOT:PSS films embedded with and without AgNWs on glass substrates show very high transmittance in the 400−1000 nm region (Figure S4, Supporting Information), which are a little lower than that of the pristine glass substrate. The high antireflective properties of AgNW-embedded PEDOT:PSS films [as indicated by the low reflectance (<30%) in the 450−1000 nm region] are observed to be beneficial in improving the HSC properties as discussed below.

A very high photovoltaic performance is achieved for the HSCs fabricated with the hybrid AgNW−IPA and AgNW−

https://dx.doi.org/10.1021/acsami.9b19400
ACS Appl. Mater. Interfaces 2020, 12, 11459−11466

EtOH films deposited on planar n-type Si/SiO_x substrates. Figure 2c,d shows the current density versus voltage ($J-V$) curves and EQE spectra of the fabricated HSCs. The photovoltaic properties of the HSCs including open-circuit voltage (V_{OC}), short-circuit current density (J_{SC}), fill factor (FF), and PCE are summarized in Table S1, Supporting Information. The highest V_{OC} of 639.0 mV (J_{SC} of 32.7 mA/cm^2 and FF of 73.4%) with a PCE of 15.3% is obtained for the best-performance AgNW−IPA cell. Similarly, a high V_{OC} of 638.4 mV (J_{SC} of 31.1 mA/cm^2 and FF of 77.4%) with a PCE of 15.4% is obtained for the best-performance AgNW−EtOH cell. An EM16-based HSC (i.e., without AgNWs) is also prepared for comparison and it shows a slightly lower V_{OC} of 630.0 mV (J_{SC} of 30.6 mA/cm^2 and FF of 74.7%) and a discernibly lower PCE of 14.4% when compared to the AgNW-embedded cells. In addition, typical diode characteristics are observed for all the solar cells measured in the dark. Similar high performance with a V_{OC} of 635 mV and a PCE of 15.2% or greater are achieved for four or more similar AgNW−IPA or AgNW−EtOH cells. The slightly higher V_{OC} for AgNW-embedded PEDOT:PSS HSCs in comparison to the EM16 cell is achieved by the reduced interface defect formation[9] and recombination, improved built-in electric field, and efficient charge transport from the interface to the top electrode (as discussed below). The EQE spectra for the AgNW-embedded HSCs also show a slightly higher efficiency in the blue (lower) wavelength region than the EM16 cell, which is in agreement with the observed improvement in the antireflective property (Figure 2b). Evidently, the reduced sheet resistance and improved antireflectance of the AgNW-embedded PEDOT:PSS films lead to the enhancement in the front carrier collection, interface carrier transport, and the solar cell performance.

The HSC efficiencies for the cells made of PEDOT:PSS embedded with thicker AgNWs (100 nm diam) using AgNW−IPA and AgNW−EtOH are higher in comparison with the highest PCE of 15% obtained for a typical cell embedded with thinner AgNWs (25 nm diam, dispersed in IPA).[23] Interestingly, the PEDOT:PSS films embedded with thicker AgNWs using AgNW−IPA and AgNW−EtOH show slightly higher sheet resistance values than PEDOT:PSS films embedded with thinner AgNWs, which is likely due to the oxidation of the thicker AgNWs. To confirm the oxidation, we collect depth-profiling XPS of Ag 3d and O 1s regions of pristine thicker AgNWs as a function of Ar ion sputtering time for 30, 60, 180, and 300 s. The Ag $3d_{5/2}$ peak for AgNWs drop-casted from IPA dispersion (designated as AgNW-I, Figure 3a) is observed at 367.4 eV (Ag $3d_{3/2}$ at 373.4 eV), which indicates a core−shell-like structure of AgNWs with an oxide layer (Ag_xO) on the peripheries.[33,34] The Ag peak is blue-shifted by 0.4 eV after 30 s of sputtering, which likely corresponds to the Ag_2O peak position after the removal of the top carbonaceous layer (arising from ambient handling). The peak is further shifted to the typical metallic Ag $3d_{5/2}$ peak position of 368.2 eV (Ag $3d_{3/2}$ at 374.2 eV) after sputtering for 60 s or more.[33,34] A slightly different trend is observed for the AgNWs drop-casted from EtOH dispersion (designated as AgNW-E, Figure 3b) with the Ag $3d_{5/2}$ peak at 367.9 eV (Ag $3d_{3/2}$ at 373.9 eV), which is 0.5 eV higher than that of the AgNW-I sample before sputtering. Sputtering for 30 s only causes the Ag $3d_{5/2}$ peak to blue-shift slightly (by ∼0.1 eV) for the AgNW-E sample. The corresponding metallic Ag $3d_{5/2}$ peak is observed at 368.2 eV (Ag $3d_{3/2}$ at 374.2 eV) after sputtering for 60 s or above,

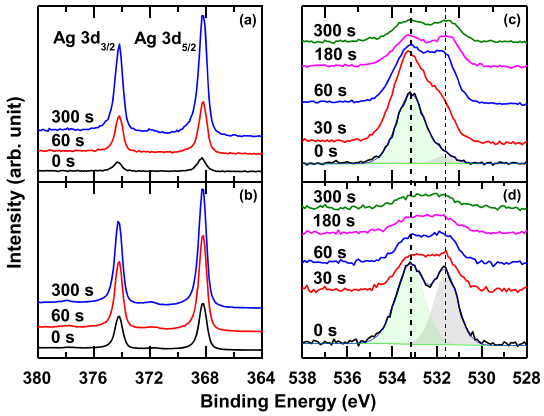

Figure 3. XPS spectra of (a,b) Ag 3d and (c,d) O 1s spectra of AgNW-I (a,c) and AgNW-E (b,d) samples and upon sputtering for 30, 60, 180, and 300 s.

similar to that observed for the AgNW-I sample. It is clear that both the AgNWs show similar metallic features after sputtering for 60 s or more, which is also in agreement with the shifts observed in the O 1s peak positions. The O 1s feature of the AgNW-I sample before sputtering (Figure 3c) shows a major peak at 532.3 eV and a weaker peak at 530.8 eV, which becomes two distinct peaks at 533.1 and 531.5 eV, respectively, after sputtering for 30 s. For the AgNW-E sample, two distinct peaks at 532.7 and 531.2 eV with nearly the same intensities are observed before sputtering (Figure 3d), and they become weakened and blue-shifted to 533.0 and 531.5 eV after sputtering for 30 s. The slight variation in the nature of this oxide layer could lead to variation in the fill factor values of the AgNW-embedded HSCs. Interestingly, both samples show two distinct O 1s features at similar positions and nearly the same relative intensities after sputtering for 60 s, and both features become further diminished upon further sputtering for 300 s. These two features are consistent with subsurface and chemisorbed oxygen species. These results suggest the presence of oxides on these thick metallic AgNWs irrespective of their dispersing solvents and indicate a core−shell structure with a Ag_xO shell covering a metallic core. The Ag_xO shell on the metallic Ag core in the AgNW-I sample comprises a mixture of AgO and Ag_2O components and the shell is mostly Ag_2O for AgNW-E. The presence of the oxide shell on AgNWs could hinder the conductivity in comparison to the thinner nanowires (25 nm diam). Indeed, depth-profiling XPS studies of the thinner AgNWs show discernibly lower extent of oxidation of the nanowires (Figure S5, Supporting Information). There is also no shift in the Ag 3d or O 1s peak positions before or after sputtering, which further confirms the presence of substantially less metallic surface oxides, which results in lower sheet resistance when mixed with PEDOT:PSS.[23] Even in the case of the thicker AgNWs, it appears that the metallic oxide is more conducting than the PEDOT:PSS itself. These oxides therefore contribute in improving the charge transfer properties of AgNW-embedded PEDOT:PSS films and ultimately the performance of HSCs.

Using the EFM mode in our AFM system, we determine the charge transfer characteristics between the AgNWs and PEDOT:PSS. Tapping-mode AFM images for the EM16, AgNW−IPA, and AgNW−EtOH films on glass substrates are shown in Figure 4a−c, respectively. The embedded AgNWs are clearly visible in their respective AFM images in Figure

https://dx.doi.org/10.1021/acsami.9b19400
ACS Appl. Mater. Interfaces 2020, 12, 11459−11466

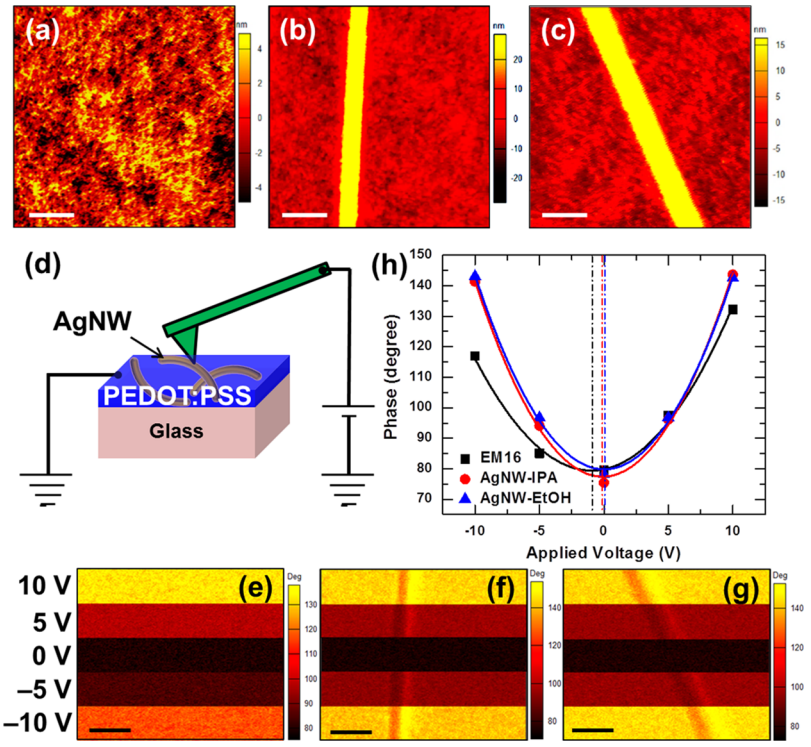

Figure 4. AFM images of (a) EM16, (b) AgNW−IPA, and (c) AgNW−EtOH films deposited on glass substrates. (d) Schematic representation of the EFM measurement method for a PEDOT:PSS film embedded with AgNWs on a glass substrate. (e−g) Corresponding EFM phase images under various biases for the EM16, AgNW−IPA, and AgNW−EtOH films, respectively. (h) Plots of the phases at five different applied biases for the EM16, AgNW−IPA, and AgNW−EtOH films. The solid lines are obtained by polynomial fittings and the dash lines represent the symmetry axis of the fitting parabola. The scale bar in the images is 600 nm.

4b,c. The EM16 sample shows a smooth surface with an estimated RMS surface roughness of 2.4 nm, which is increased to 14.1 nm for the AgNW−IPA sample and to 15.2 nm for the AgNW−EtOH sample because of the presence of the AgNWs. Figure 4d demonstrates the typical EFM testing method with the films (deposited on glass substrates) grounded during the measurement. A bias voltage (from −10 to 10 V with an increment of 5 V) is applied to the tip during the EFM measurement to allow extraction of the Coulombic force.[35,36] The resulting phase shift maps obtained with the five different applied bias voltages over the same sample area as the AFM measurement are combined into a single image for comparison (Figure 4e−g). The left-axis labels in Figure 4e indicate the applied bias voltages used for the acquired images, appropriately selected stripes of which are used for the combined image. The EFM phase images of nanowires-embedded PEDOT:PSS show a well-resolved nanowire at higher applied biases (±5 and ±10 V), while EM16 shows slightly higher degrees of phase shift with positive biases than the respective negative biases. For the EM16 film, an applied bias of 10 V shows a higher phase shift of slightly above 130°, while the same applied bias voltage in the opposite polarity gives a phase shift below 120°. Both AgNW-embedded films exhibit high phase shifts of above 140° at the higher applied biases of ±10 V. The changes in the phase shift degree for the EM16, AgNW−IPA, and AgNW−EtOH samples are summarized in Figure 4h. It is known that the negative shift of the symmetry axis of the fitting parabola indicates negative charges at the surface and vice versa.[36] The fitted curve of the EM16 film shows that the symmetry axis is located at a bias voltage of −1.5 V. This small offset from the zero bias voltage is in accord with the electron affinity of the PEDOT:PSS. The fitted curves of the AgNW−IPA and AgNW−EtOH samples show their corresponding symmetry axes to be near 0 V (Figure 4h), which indicates the effective improvement in the charge transfer between AgNWs and PEDOT:PSS and therefore the reduced electron affinity of the sample surface.

Further analysis of the topography and charge transfer characteristics of the EM16 and AgNW−IPA samples (Figure 5a,b) is performed by obtaining the respective height and phase profiles along selected linescans across the image area. The height profile of the EM16 sample confirms its generally smooth surface (Figure 5c). On the other hand, a step height of about 60 nm is found in the height profile for the AgNW−IPA film (Figure 5d), indicating that the AgNW diameter is larger than the film thickness and the AgNWs therefore cause the increased surface roughness of the film. Similar observation can also be made for the other AgNW-embedded PEDOT:PSS film (AgNW−EtOH). It should be noted that the thickness of the PEDOT:PSS film (without AgNWs) is about 85 nm and for the AgNW-embedded PEDOT:PSS films the thickness is higher (by ∼60 nm) at the locations of the AgNWs. Because the EFM phase images are acquired at a selected tip bias with the tip withdrawn, the phase images are mainly affected by the charge transfer properties of the sample surface. An increase in the phase profile is observed at the location of the nanowire for the AgNW-embedded samples, and this phase increase is found to increase with increasing tip bias. This change in the phase signature can be attributed to the enhanced charge transfer with the AgNWs. The slight dip in the phase linescan on one side of the nanowire is caused by a topographical crosstalk effect (which is related to the direction of the tip

https://dx.doi.org/10.1021/acsami.9b19400
ACS Appl. Mater. Interfaces 2020, 12, 11459−11466

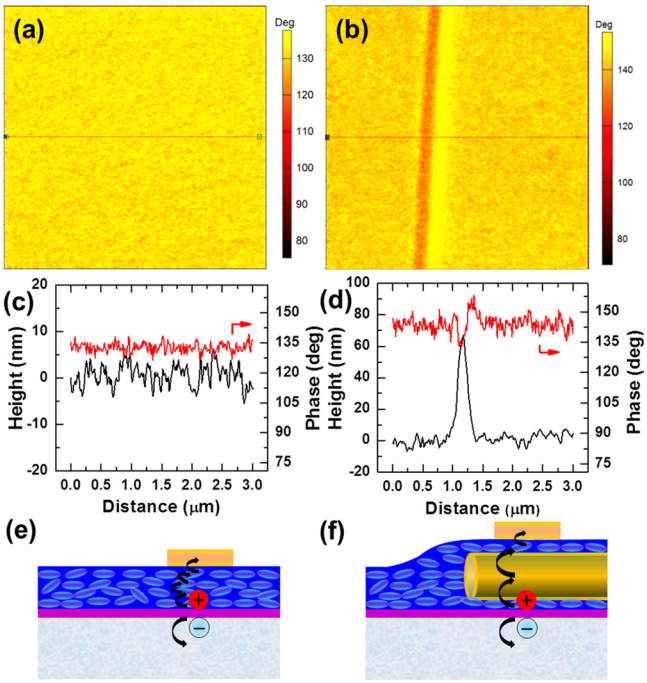

Figure 5. (a,b) EFM images obtained at an applied bias of 10 V and (c,d) height profiles of the AFM image (black) and phase profiles of the corresponding EFM images (red), obtained along the respective linescans marked in (a,b), for (a,c) EM16 and (b,d) AgNW−IPA samples. Schematic representations of the charge transfer process in typical HSCs made of (e) EM16 and (f) AgNW-embedded PEDOT:PSS samples. The charge transfer in EM16 occurs through the conducting PEDOT grains (represented by ovals), and that in the AgNW−IPA or AgNW−EtOH samples occurs from PEDOT grains to AgNWs and then from the AgNWs to the grains, and finally to the top silver electrode.

scan) in the EFM phase signal. This EFM study illustrates the charge transfer modification in hybrid and heterostructure electronic systems and such an effect can also be applied to other similar systems.

The consequence of embedding these AgNWs with a diameter larger than the PEDOT:PSS film thickness triggers modifications in the film morphology, which is schematically illustrated in Figure 5e,f. For the EM16 sample, the reduction of the coil-like benzoid structures and formation of extended quinoid structures in the ellipsoidal PEDOT grains are known to be caused by the mixed cosolvent addition to PEDOT:PSS, and these changes lead to a highly conductive thin film. In addition, the separation and removal of PSS from PEDOT during the spin-coating process is facilitated by methanol in the mixed cosolvent (EM) solution. As the EG in the mixed cosolvent stabilizes the extended quinoid structures in the PEDOT:PSS matrix, the remaining insulating PSS in the film is expected to segregate to the voids among the grains, which leads to a more closely packed matrix of highly conducting PEDOT grains. For an AgNW-embedded PEDOT:PSS film, the nanowires are embedded in a layer of highly conducting PEDOT grains and the charge transfer takes place from the grains to the Ag metal core through the conductive Ag_xO shell of the AgNW and then to other grains before reaching the electrodes. Along with the improved antireflective property and reduced sheet resistance, this more efficient charge transfer process enhances the properties of HSCs. This has made possible a very high V_{OC} of 639.0 mV and a high J_{SC} of 32.7 mA/cm^2, with the PCE reaching greater than 15.3% for the planar cells.

CONCLUSIONS

In summary, we characterize the charge transfer properties of AgNW-embedded PEDOT:PSS by using EFM analysis. The HSC made from a hybrid AgNW-embedded PEDOT:PSS film (AgNW−IPA) on a planar silicon substrate shows a very high V_{OC} of 639 mV and a very high PCE of 15.3%. Different dispersing solvents for the AgNWs only slightly influence the overall properties of PEDOT:PSS and its charge transfer characteristics as observed from the EFM studies. In addition, we do not observe any significant effect of these dispersing solvents (IPA and EtOH) on the impressive HSC properties themselves. Indeed, the PCEs greater than 15.3% achieved for both AgNW-embedded PEDOT:PSS-based HSCs in this work are among the highest efficiencies ever reported for planar single-junction HSCs. This is even more remarkable considering that this high PCE is obtained without the use of any top antireflective coating, interface engineering, and complex fabrication processes. Further enhancement in the HSC properties can clearly be achieved by these additional fabrication processes such as PEDOT:PSS post surface treatments, antireflective coating, and interface modifications. The present method of producing hybrid metallic nanowire-embedded PEDOT:PSS with efficient charge transfer properties can be incorporated into organic−organic or organic−inorganic electronic devices other than HSCs to further advance their performance, and the EFM analysis method could also be used to study the charge transfer characteristics in other similar systems at high spatial resolution.

ASSOCIATED CONTENT

Supporting Information

The Supporting Information is available free of charge at https://pubs.acs.org/doi/10.1021/acsami.9b19400.

Schematic structure representations of PEDOT:PSS, cosolvents, and prepared solutions, SEM and TEM images of AgNWs dispersed in EtOH, low magnification SEM images of AgNWs dispersed in IPA and ETOH, transmittance spectra of AgNW−IPA, AgNW−EtOH, and EM16 films on glass substrates along with the pristine glass substrate, depth profile XPS Ag 3d and O 1s spectra of 25 nm diameter AgNWs dispersed in IPA, and a table summarizing sheet resistance and solar cell properties of the samples (PDF)

AUTHOR INFORMATION

Corresponding Author

Kam Tong Leung − *WATLab and Department of Chemistry, University of Waterloo, Waterloo, Ontario N2L3G1, Canada;* orcid.org/0000-0002-1879-2806; Email: tong@uwaterloo.ca

Authors

Joseph P. Thomas − *WATLab and Department of Chemistry, University of Waterloo, Waterloo, Ontario N2L3G1, Canada;* orcid.org/0000-0001-6455-908X

Qiuyu Shi − *WATLab and Department of Chemistry, University of Waterloo, Waterloo, Ontario N2L3G1, Canada*

Marwa Abd-Ellah − *WATLab and Department of Chemistry, University of Waterloo, Waterloo, Ontario N2L3G1, Canada*

https://dx.doi.org/10.1021/acsami.9b19400
ACS Appl. Mater. Interfaces 2020, 12, 11459−11466

Lei Zhang − *WATLab and Department of Chemistry, University of Waterloo, Waterloo, Ontario N2L3G1, Canada*
Nina F. Heinig − *WATLab and Department of Chemistry, University of Waterloo, Waterloo, Ontario N2L3G1, Canada*

Complete contact information is available at: https://pubs.acs.org/10.1021/acsami.9b19400

Notes

The authors declare no competing financial interest.

■ ACKNOWLEDGMENTS

This work was supported by the Natural Sciences and Engineering Research Council of Canada.

■ REFERENCES

(1) Um, H.-D.; Choi, D.; Choi, A.; Seo, J. H.; Seo, K. Embedded Metal Electrode for Organic-Inorganic Hybrid Nanowire Solar Cells. *ACS Nano* **2017**, *11*, 6218−6224.
(2) Zhang, Y.; Cui, W.; Zhu, Y.; Zu, F.; Liao, L.; Lee, S.-T.; Sun, B. High Efficiency Hybrid PEDOT:PSS/nanostructured Silicon Schottky Junction Solar Cells by Doping-Free Rear Contact. *Energy Environ. Sci.* **2015**, *8*, 297−302.
(3) Zhu, J.; Yang, X.; Yang, Z.; Wang, D.; Gao, P.; Ye, J. Achieving a Record Fill Factor for Silicon−Organic Hybrid Heterojunction Solar Cells by Using a Full-Area Metal Polymer Nanocomposite Top Electrode. *Adv. Funct. Mater.* **2018**, *28*, 1705425.
(4) Xia, Z.; Gao, P.; Sun, T.; Wu, H.; Tan, Y.; Song, T.; Lee, S.-T.; Sun, B. Buried MoOx/Ag Electrode Enables High-Efficiency Organic/Silicon Heterojunction Solar Cells with a High Fill Factor. *ACS Appl. Mater. Interfaces* **2018**, *10*, 13767−13773.
(5) He, J.; Gao, P.; Yang, Z.; Yu, J.; Yu, W.; Zhang, Y.; Sheng, J.; Ye, J.; Amine, J. C.; Cui, Y. Silicon/Organic Hybrid Solar Cells with 16.2% Efficiency and Improved Stability by Formation of Conformal Heterojunction Coating and Moisture-Resistant Capping Layer. *Adv. Mater.* **2017**, *29*, 1606321.
(6) Ugur, A.; Katmis, F.; Li, M.; Wu, L.; Zhu, Y.; Varanasi, K. K.; Gleason, K. K. Low-Dimensional Conduction Mechanisms in Highly Conductive and Transparent Conjugated Polymers. *Adv. Mater.* **2015**, *27*, 4604−4610.
(7) Wang, H.-P.; Lin, T.-Y.; Tsai, M.-L.; Tu, W.-C.; Huang, M.-Y.; Liu, C.-W.; Chueh, Y.-L.; He, J.-H. Toward Efficient and Omnidirectional N-Type Si Solar Cells: Concurrent Improvement in Optical and Electrical Characteristics by Employing Microscale Hierarchical Structures. *ACS Nano* **2014**, *8*, 2959−2969.
(8) Thomas, J. P.; Zhao, L.; McGillivray, D.; Leung, K. T. High-Efficiency Hybrid Solar Cells by Nanostructural Modification in PEDOT:PSS with Co-Solvent Addition. *J. Mater. Chem. A* **2014**, *2*, 2383−2389.
(9) Thomas, J. P.; Leung, K. T. Defect-Minimized PEDOT:PSS/planar-Si Solar Cell with Very High Efficiency. *Adv. Funct. Mater.* **2014**, *24*, 4978−4985.
(10) Zhang, W.; Zhao, B.; He, Z.; Zhao, X.; Wang, H.; Yang, S.; Wu, H.; Cao, Y. High-Efficiency ITO-Free Polymer Solar Cells Using Highly Conductive PEDOT:PSS/surfactant Bilayer Transparent Anodes. *Energy Environ. Sci.* **2013**, *6*, 1956.
(11) Crispin, X.; Jakobsson, F. L. E.; Crispin, A.; Grim, P. C. M.; Andersson, P.; Volodin, A.; van Haesendonck, C.; Van der Auweraer, M.; Salaneck, W. R.; Berggren, M. The Origin of the High Conductivity of (PEDOT-PSS) Plastic Electrodes. *Chem. Mater.* **2006**, *18*, 4354−4360.
(12) Thomas, J. P.; Leung, K. T. Mixed Co-Solvent Engineering of PEDOT:PSS to Enhance Its Conductivity and Hybrid Solar Cell Properties. *J. Mater. Chem. A* **2016**, *4*, 17537−17542.
(13) Sharma, M.; Pudasaini, P. R.; Ruiz-Zepeda, F.; Elam, D.; Ayon, A. A. Ultrathin, Flexible Organic−Inorganic Hybrid Solar Cells Based on Silicon Nanowires and PEDOT:PSS. *ACS Appl. Mater. Interfaces* **2014**, *6*, 4356−4363.
(14) Kim, N.; Kee, S.; Lee, S. H.; Lee, B. H.; Kahng, Y. H.; Jo, Y.-R.; Kim, B.-J.; Lee, K. Highly Conductive PEDOT:PSS Nanofibrils Induced by Solution-Processed Crystallization. *Adv. Mater.* **2014**, *26*, 2268−2272.
(15) McGillivray, D.; Thomas, J. P.; Abd-Ellah, M.; Heinig, N. F.; Leung, K. T. Performance Enhancement by Secondary Doping in PEDOT:PSS/Planar-Si Hybrid Solar Cells. *ACS Appl. Mater. Interfaces* **2016**, *8*, 34303−34308.
(16) Kim, N.; Kang, H.; Lee, J.-H.; Kee, S.; Lee, S. H.; Lee, K. Highly Conductive All-Plastic Electrodes Fabricated Using a Novel Chemically Controlled Transfer-Printing Method. *Adv. Mater.* **2015**, *27*, 2317−2323.
(17) Li, Q.; Yang, J.; Chen, S.; Zou, J.; Xie, W.; Zeng, X. Highly Conductive PEDOT:PSS Transparent Hole Transporting Layer with Solvent Treatment for High Performance Silicon/Organic Hybrid Solar Cells. *Nanoscale Res. Lett.* **2017**, *12*, 506.
(18) Wei, Q.; Mukaida, M.; Naitoh, Y.; Ishida, T. Morphological Change and Mobility Enhancement in PEDOT:PSS by Adding Co-Solvents. *Adv. Mater.* **2013**, *25*, 2831−2836.
(19) Louarn, G.; Trznadel, M.; Buisson, J. P.; Laska, J.; Pron, A.; Lapkowski, M.; Lefrant, S. Raman Spectroscopic Studies of Regioregular Poly (3-Alkylthiophenes). *J. Phys. Chem.* **1996**, *100*, 12532−12539.
(20) Garreau, S.; Louarn, G.; Buisson, J. P.; Froyer, G.; Lefrant, S. In Situ Spectroelectrochemical Raman Studies of Poly(3,4-Ethylenedioxythiophene) (PEDT). *Macromolecules* **1999**, *32*, 6807−6812.
(21) Thomas, J. P.; Srivastava, S.; Zhao, L.; Abd-Ellah, M.; McGillivray, D.; Kang, J. S.; Rahman, M. A.; Moghimi, N.; Heinig, N. F.; Leung, K. T. Reversible Structural Transformation and Enhanced Performance of PEDOT:PSS-Based Hybrid Solar Cells Driven by Light Intensity. *ACS Appl. Mater. Interfaces* **2015**, *7*, 7466−7470.
(22) Chen, T.-G.; Huang, B.-Y.; Liu, H.-W.; Huang, Y.-Y.; Pan, H.-T.; Meng, H.-F.; Yu, P. Flexible Silver Nanowire Meshes for High-Efficiency Microtextured Organic-Silicon Hybrid Photovoltaics. *ACS Appl. Mater. Interfaces* **2012**, *4*, 6857−6864.
(23) Thomas, J. P.; Rahman, M. A.; Srivastava, S.; Kang, J.-S.; McGillivray, D.; Abd-Ellah, M.; Heinig, N. F.; Leung, K. T. Highly Conducting Hybrid Silver-Nanowire-Embedded Poly(3,4-ethylenedioxythiophene):Poly(styrenesulfonate) for High-Efficiency Planar Silicon/Organic Heterojunction Solar Cells. *ACS Nano* **2018**, *12*, 9495−9503.
(24) Kim, Y.-S.; Chang, M.-H.; Lee, E.-J.; Ihm, D.-W.; Kim, J.-Y. Improved Electrical Conductivity of PEDOT-Based Electrode Films Hybridized with Silver Nanowires. *Synth. Met.* **2014**, *195*, 69−74.
(25) Kim, S.; Kim, S. Y.; Kim, J.; Kim, J. H. Highly Reliable AgNW/PEDOT:PSS Hybrid Films: Efficient Methods for Enhancing Transparency and Lowering Resistance and Haziness. *J. Mater. Chem. C* **2014**, *2*, 5636.
(26) Xu, Q.; Song, T.; Cui, W.; Liu, Y.; Xu, W.; Lee, S.-T.; Sun, B. Solution-Processed Highly Conductive PEDOT:PSS/AgNW/GO Transparent Film for Efficient Organic-Si Hybrid Solar Cells. *ACS Appl. Mater. Interfaces* **2015**, *7*, 3272−3279.
(27) Yoon, S.-S.; Khang, D.-Y. High Efficiency (>17%) Si-Organic Hybrid Solar Cells by Simultaneous Structural, Electrical, and Interfacial Engineering via Low-Temperature Processes. *Adv. Energy Mater.* **2018**, *8*, 1702655.
(28) He, J.; Wan, Y.; Gao, P.; Tang, J.; Ye, J. Over 16.7% Efficiency Organic-Silicon Heterojunction Solar Cells with Solution-Processed Dopant-Free Contacts for Both Polarities. *Adv. Funct. Mater.* **2018**, *28*, 1802192.
(29) Liu, Z.; Yang, Z.; Wu, S.; Zhu, J.; Guo, W.; Sheng, J.; Ye, J.; Cui, Y. Photoinduced Field-Effect Passivation from Negative Carrier Accumulation for High-Efficiency Silicon/Organic Heterojunction Solar Cells. *ACS Nano* **2017**, *11*, 12687−12695.
(30) Liu, Q.; Ishikawa, R.; Funada, S.; Ohki, T.; Ueno, K.; Shirai, H. Highly Efficient Solution-Processed Poly(3,4-Ethylenedioxythiophene):Poly(styrenesulfonate)/Crystalline-Silicon Heterojunc-

tion Solar Cells with Improved Light-Induced Stability. *Adv. Energy Mater.* **2015**, *5*, 1500744.
(31) Yang, Z.; Gao, P.; He, J.; Chen, W.; Yin, W.-Y.; Zeng, Y.; Guo, W.; Ye, J.; Cui, Y. Tuning of the Contact Properties for High Efficiency Si/PEDOT:PSS Heterojunction Solar Cells. *ACS Energy Lett.* **2017**, *2*, 556−562.
(32) Liu, J.; Ji, Y.; Liu, Y.; Xia, Z.; Han, Y.; Li, Y.; Sun, B. Doping-Free Asymmetrical Silicon Heterocontact Achieved by Integrating Conjugated Molecules for High Efficient Solar Cell. *Adv. Energy Mater.* **2017**, *7*, 1700311.
(33) Weaver, J. F.; Hoflund, G. B. Surface Characterization Study of the Thermal Decomposition of Ag_2O. *J. Phys. Chem.* **1994**, *98*, 8519−8524.
(34) Kaspar, T. C.; Droubay, T.; Chambers, S. A.; Bagus, P. S. Spectroscopic Evidence for Ag(III) in Highly Oxidized Silver Films by X-Ray Photoelectron Spectroscopy. *J. Phys. Chem. C* **2010**, *114*, 21562−21571.
(35) Hassenkam, T.; Greve, D. R.; Bjørnholm, T. Direct Visualization of the Nanoscale Morphology of Conducting Polythiophene Monolayers Studied by Electrostatic Force Microscopy. *Adv. Mater.* **2001**, *13*, 631−634.
(36) Tu, B.; Shao, Y.; Chen, W.; Wu, Y.; Li, X.; He, Y.; Li, J.; Liu, F.; Zhang, Z.; Lin, Y.; Lan, X.; Xu, L.; Shi, X.; Ng, A. M. C.; Li, H.; Chung, L. W.; Djurišić, A. B.; He, Z. Novel Molecular Doping Mechanism for N-Doping of SnO_2 via Triphenylphosphine Oxide and Its Effect on Perovskite Solar Cells. *Adv. Mater.* **2019**, *31*, 1805944.

https://dx.doi.org/10.1021/acsami.9b19400
ACS Appl. Mater. Interfaces 2020, 12, 11459−11466